Small Amphiphilic Organics, Coordination Extended Solids, and Constant Curvature Structures†

STEPHEN LEE,* ABHIJIT BASU MALLIK, ZHENGTAO XU, EMIL B. LOBKOVSKY, AND LIEU TRAN

Department of Chemistry and Chemical Biology, Baker Laboratory, Cornell University, Ithaca, New York 14853-1301

Received June 17, 2004

ABSTRACT

In this Account, we explore the role constant curvature structures play in amphiphilic small molecule crystals and extended coordination solids. A constant curvature structure is one in which there is a surface or interface that has the same curvature throughout its surface. Simple examples of such structures contain spheres (micelles), columns, or layers. Yet another family are cubic as is found in the gyroid topology. For amphiphilic systems, there are two domains, one generally hydrophobic and the other hydrophilic. We find that the interfaces between these two domains in small molecule structures resemble those in larger scale systems and adopt topologies related to constant curvature structures. The hydrophobic-to-total volume ratio, a molecular parameter, can be used to predict which type of constant curvature structure is adopted. In the case of three coordinate extended solids, constant curvature plays a role both in the extended net topology and in the hydrophobic-to-hydrophilic interface.

Introduction

The rationalization and prediction of crystal structure has proven to be a difficult sticking point in the field of molecular architecture.[1−3] The difficulty lies in the large number of intermolecular interactions with similar energetic magnitude.[4,5] The result is that tiny perturbations in molecular constituents can lead to global changes in the overall crystal packing. As a result, in only a limited number of cases have chemists been able to a priori deduce from knowledge of the chemical composition alone the actual crystal structure of a chemical system.[6] As a further sad consequence, the optimization of materials properties, a process that often requires control of the overall crystal structure, at times devolves into a hit-or-miss activity rather than an exact scientific endeavor.

In very large systems, where the vagaries of individual energetic terms are often averaged away, the situation is simpler. In block copolymers with unit cells approaching 1000 Å,[7,8] lyotropic amphiphilic systems of similar dimensions,[9] large inorganic systems,[3,10,11] or biological cells themselves,[12−14] scientists find crystals with just a few simple topologies. Here, among the most common crystalline topologies are the spherical (*s*), columnar (*c*), lamellar (*l*), and cubic bicontinuous (*bi*) structures (the bicontinuous topology has exactly two separate continuous three-dimensional domains). Prototypes of these structures are illustrated in Figure 1.

As Figure 1 shows, there is a commonality between these structures. In each case, there are two types of domains and a well defined interface between them. The interfaces are of a particular nature. In each interface, the mean curvature is constant everywhere (the mean curvature is defined for each point of a surface; it is the sum of the curvature of the two surface principal axes). In two of the structure types, the lamellar and cubic bicontinuous topologies, the mean curvature is not only constant, but it is formally zero. In Figure 1, we illustrate this for one of the most beautiful of all cubic bicontinuous structures, the gyroid topology.[14] As this figure shows, every point of the surface is a saddle point with everywhere equal and opposite curvature of the two principal axes.

In this Account, we see how these simple structures evolve as we turn from large length-scale systems to decreasingly small molecules. For chemical formulations with two clearly distinguishable (and immiscible) chemical components, the above-described topologies are maintained and clear interfaces are found even when the molecular domains approach 5−10 Å in length. We have discovered that this structural evolution allows the prediction of overall crystalline topology.

We explore further ramifications of constant curvature structures in the field of coordination extended solids. Here we see that coordination extended solids with tritopic trigonal planar ligands and three coordinate metal atoms frequently adopt constant curvature structures. The most common topology is the lamellar topology. But the gyroid topology is also found. In such cases, the gyroid interface can often be related to the position of either the counterions themselves or the interface between the counterions and the organic−metal framework.

Stephen Lee's mentors are Jeremy Burdett, Greg Hillhouse, Jean Rouxel, and Wolfgang Jeitschko. Since 1998, he has served as a professor of chemistry and chemical biology at Cornell University, Ithaca, NY. His interests include large length scale intermetallic and small length scale organic crystal structures.

Abhijit Basu Mallik received his Ph.D. from Cornell University (2004) and his M.Sc. from Indian Institute of Technology, Kanpur (1998). At present, he is with the group of Professor Zhenan Bao at Stanford University as a Postdoctoral Scholar. His research interest lies in organic materials chemistry.

Zhengtao Xu obtained his Ph.D. at Cornell University (2001) and did postdoctoral work with David B. Mitzi at IBM T. J. Watson Research Center. Currently an assistant professor at George Washington University, he is interested in combining organic synthesis and solid state chemistry with a focus on solution-processible hybrid semiconductors.

† This paper is dedicated to the memory of Prof. Dr. rer. nat. Peter Böttcher (1939-2003).

* To whom correspondence should be addressed. E-mail: sl137@cornell.edu.

Emil B. Lobkovsky, born in the former USSR, received his M.Sc. in Physics from Gorky State University and Ph.D. in Chemistry from Moscow State University in 1974. He is now a cyrstallographer at the Cornell Chemistry Department.

Lieu Tran, born in Dong Nai, Vietnam, received her B.A. in Neurobiology from Cornell University in 2004. She plans to enroll in medical school in the near future.

10.1021/ar0401653 CCC: $30.25
Published on Web 03/15/2005

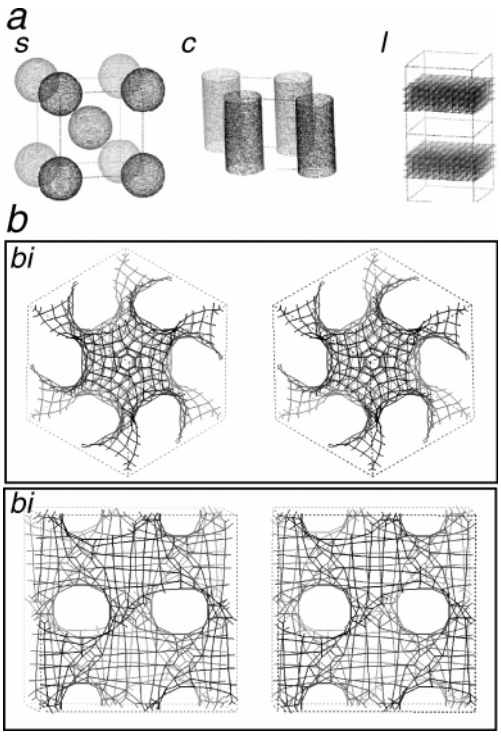

FIGURE 1. The spherical (*s*), columnar (*c*), and lamellar (*l*) topologies (a) and stereoviews (b) of the cubic bicontinuous (*bi*) gyroid topology along (top) the [1 1 1] direction and (bottom) the [1 0 0] direction. The *s*, *c*, and *l* surfaces all have constant curvature (for *l*, curvature is zero). In the *bi* topology, every surface point is a saddle point. For these saddle points the curvature of the principal axes are equal in magnitude and opposite in sign. Mean curvature is therefore zero. The *bi* surface is therefore a constant curvature surface.

Hydrophobic-to-Total Volume Ratios

The relatively small number of constant curvature structure types found in a large and disparate number of fields has led to the development of simple and seemingly universal structural models.[7−9,15] In this endeavor, two variables have come to the fore. Both variables are based on the observation that across fields, the actual chemical systems often contain two rather immiscible components. These two components, one often relatively hydrophobic and the other hydrophilic, are forced into contact with one another (for example, by a surfactant molecule or, as in block copolymers, by a covalent bond that attaches the two components to one another). As a result, the crystal structure contains two domains with a high free energy interface between them. This high free energy surface relates to one of the variables, χN (χ is the Flory−Huggins interaction parameter;[16] N is the number of monomer units in the polymer). For a high χN value, the free energy between the two domains is large, surface area between domains tends to minimize, and constant curvature structures often result.

The second variable also has its origin in the high free energy of the surface. Some thought shows that if one of the components is a minor component, then it will form a spherical impurity inside the major component. If on the other hand the two components are equal in amount, minimization of the surface area between the components will lead to a lamellar structure with alternating layers. The key variable is the volume ratio between components. Because the two components have often different hydrophobicities, this variable can be expressed as the hydrophobic-to-total volume ratio.

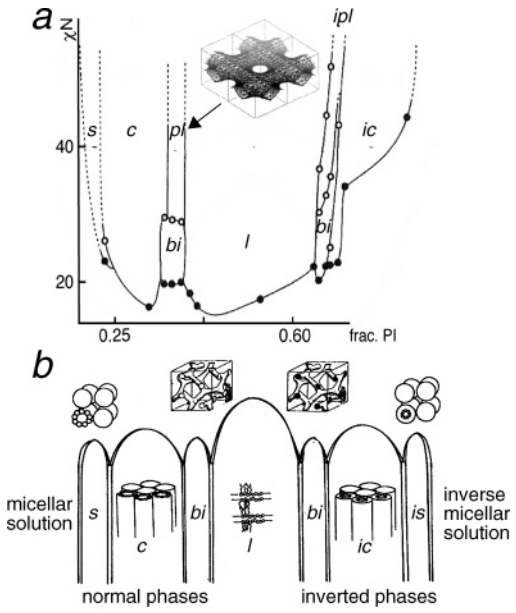

FIGURE 2. Phase diagram for (a) polystyrene (PS)−polyisoprene (PI) diblock copolymer[8] as a function of PS-to-total volume ratio and (b) generalized lyotropic liquid crystals as a function of hydrophobic-to-total volume ratio;[9] *s* = spheres; *c* = columns; *l* = layers; *bi* = bicontinuous; *pl* = perforated layers; *is* = inverted spheres; *ic* = inverted columns; *ipl* = inverted perforated layers.

Figure 2a shows, for polystyrene−polyisoprene block copolymers, the actual evolution in structure type as a function of both χN and this volume ratio.[8] As this figure shows, there are only five different crystalline topologies, the four previously mentioned constant curvature structures, and one more structure, found for high χN values, the perforated layer (*pl*) topology. This last topology is described well by its name and is illustrated in the figure.

As this figure shows, the hydrophobic-to-total volume ratio differentiates well the different structure types. At low polyisoprene-to-total volume ratios, the spherical phase is found; at slightly higher values, the columnar phase is most stable, followed by the cubic bicontinuous and lamellar phase. For higher volume ratios still, the polystyrene becomes the minority component. Here, these phase types repeat themselves, albeit in reverse order, evolving from bicontinuous to columnar and finally, at very high hydrophobic-to-total volume ratios, to a spherical phase. In these latter phases, polystyrene is contained within the perforated layers, columns, or spheres themselves: these phases are referred to as inverse phases (inverted spherical (*is*), inverted columnar (*ic*), and inverted perforated layer (*ipl*)).[17]

In Figure 2b, we show a similar plot from the lyotropic liquid crystal literature.[9] The diagram is suprisingly similar to the block copolymer diagram. The same constant curvature phases are found (*s*, *c*, *bi*, *l*, *bi*, *ic*, and *is*) at roughly the same hydrophobic-to-total volume ratios.

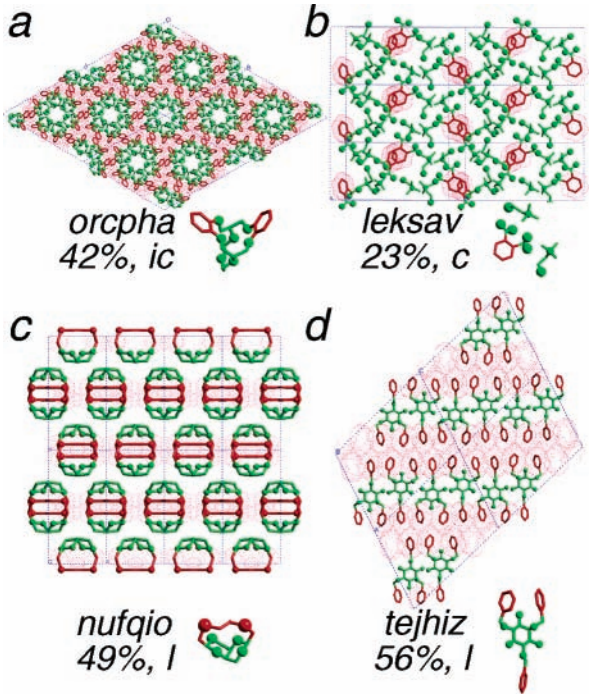

FIGURE 3. Crystal structures of (a) *orcpha*,[19] (b) *leksav*,[20] (c) *nufqio*,[21] and (d) *tejhiz*.[22] Hydrophobic and hydrophilic moieties are illustrated in red and green, respectively: large green spheres, oxygen atoms; small green spheres, nitrogen atoms; red spheres, sulfur atoms; red hydrophobic portion of crystal, stippled shading. Included are the CSD entry codes, hydrophobic-to-total volume fractions, molecular structures, and topological types.

Because the perforated layer structure is not included, no reference to a surface free energy, like χN, is required.

The similarity between panels a and b of Figure 2 suggests that, for two-component, large length scale systems with a high free energy between components, there is a universal phase diagram. The focus of this Account, however, is not whether such a universal diagram exists; rather, it is whether the same structural patterns hold for small molecule systems as well. We turn first to the Cambridge Structural Database (CSD) to answer this question.

This database is rich in structures, but to examine the utility of phase diagrams such as those shown in Figure 2, we need algorithms that determine both hydrophobic-to-total volume ratio and structure type for small molecule crystals. The algorithms that we choose are based on the van der Waals radii of the atoms. To determine the hydrophobic-to-total volume ratio, we use these radii to ascribe the volume of hydrophobic and hydrophilic molecular fragments; these volumes then taken together give the hydrophobic-to-total volume ratio.

We also use these radii to determine the structural topology of a given crystal. In particular, we use these radii (or rather 1.15−1.30 × the van der Waals radii[18]) to determine which moieties are in close contact with one another. From these close contacts, we determine the structure type. We note spheres, columns, and perforated layers are zero-, one-, and two-dimensional fragments contained in a three-dimensional matrix. (These columns and perforated layers are all parallel). Bicontinuous systems have two, and only two, three-dimensional components, while the lamellar structure has alternating parallel two-dimensional sheets. The dimensionality of the close contacts therefore determines the topology of the system (exact procedures are given in Supporting Information).

Table 1. Correlation between Structure Types[a] and Hydrophobic-to-Total Volume Ratios

vol ratios (%)	*s* and *c*	*pl*	*bi* and *l*	*ipl*	*ic* and *is*
0−10	1				
10−20	2				
20−30	14		3		
30−40	10	3	10		
40−50	1	6	35		1
50−60			12	5	1
60−70			1	2	0
70−80					6
80−90					2
90−100					1

[a] Structural classification based on closest contacts defined as less than 1.30 times the sum of the van der Waals radii.

Using these definitions, we considered first four classes of CSD crystals: aromatic polyethers (and polyalcohols), aromatic ammonium carboxylates, cyclohexylammonium carboxylates, and ether-thioethers (see Supporting Information). In each class, molecules have two components, one hydrophobic (or soft) and the other hydrophilic (or hard). Using the above algorithms, we determined the volume ratios and topologies of 120 systems. Of these, 116 belonged to the above-mentioned phase types.

That so many phases have topologies such as those in Figure 2 suggests the utility of the above structural classification. However attention should be paid to the actual interfaces themselves. We need to see whether for small molecule systems the interfaces remain smooth and whether their curvature is constant. In prior publications, we have illustrated all 120 crystal structures (see Supporting Information). Here we limit ourselves to just four of the systems, two columnar and two lamellar, see Figure 3. However, the points made here apply to the full data set as well.

The *c* phases, referring to their CSD entry code, are *orcpha*,[19] an aromatic polyether, and *leksav*,[20] an aromatic ammonium carboxylate (the molecules are illustrated in Figure 3). In both cases, the aromatic portions of the molecules aggregate together in columnar bundles, and these columns are embedded in a hydrophilic matrix. The columns are parallel with one another, and in both cases, each column has six neighboring columns. In the case of *orcpha*, the result is a hexagonal structure; the more common case is shown in *leksav*: here the columns are pseudohexagonally distributed. The relation between these two structures and the true hexagonal *c* phase illustrated in Figures 1 and 2 is clear.

The two *l* structures illustrated in Figure 3 are *nufqio*,[21] a thioether, and *tejhiz*,[22] an aromatic polyether polyalcohol. As *nufqio* shows, the soft thioether moieties of different molecules aggregate together, as do neighboring ether groups. The result of this aggregation is that both the ether and the thioether domains form lamellar sheets

with a clear flat interface between them. An equally clear interface can be found between the hydrophobic aromatic portions and the relatively hydrophilic polyether polyalcohol portions of *tejhiz*. In this latter case, the molecule is triangularly shaped. These triangles come together in a head-to-tail fashion to create a clean hydrophobic-to-hydrophilic interface.

Taken together, these four examples suggest the qualitative ability of constant curvature structures in rationalizing small molecule amphiphilic architectures. But the results in Figure 2 suggest that the hydrophobic-to-total volume may have a quantitative role as well. In particular, the *s* and *c* phases are found at volume ratios of 15−32%, the *bi* and *pl* phase at 32−37%, the *l* structure at 37−62%, the *ipl* and *bi* at 62−67%, and finally the *ic* and *is* topologies at 67−85%.

In Table 1, for the 120 systems, we show the topology as a function of this same hydrophobic-to-total volume ratio. In this table, we group together the *s* and *c* structures, the *l* and *bi* topologies, and the *ic* and *is* types. With this grouping, Table 1 reveals that topologies divide well along lines of hydrophobic-to-total volume ratios. At 20−30%, the *s* and *c* topology is most common, while the *l* and *bi* phases predominate for volume ratios of 40−50%. At very high volume ratios, one finds the *ic* and *is* topologies. Finally, the *pl* or *ipl* phases are found at volume ratios intermediate between, respectively, the *s* and *c* or *is* and *ic* structures and the *bi* or *l* topologies.

The boundaries of Table 1 are less sharp than the boundaries of Figure 2. In part, this is because Table 1 is the tabulation of many different systems belonging to a range of amphiphilic classes. But the presence of idiosyncratic local intermolecular forces must also play a role. One consequence of the diffuse boundaries of Table 1 is that the two separate regions attributed to the *bi* phase in Figure 2 have merged into a single domain. This domain overlaps with the *l* region, and for this reason, the two structure types are placed in the same category in Table 1. Table 1 and Figure 2 suggest that constant curvature structures play a role in small molecule systems, as well as large-length-scale systems.

Topology Predictions for Small Molecule Amphiphiles

These results suggest that the hydrophobic-to-total volume ratio can be used to predict the topologies of small molecule crystals (volume ratio can be calculated from a knowledge of the molecule itself). Looking at Table 1, we predict that three-quarters of all molecules with a volume ratio of 40−50% will have the *l* or *bi* topology, and similarly molecules with volume ratios of 20−30% will be in the *c* and *s* families.

Testing the accuracy of predictions requires a little care. The simplest procedure is to publish after one has tested in the laboratory the accuracy of the predictions. However, because it is hard to publish incorrect predictions, the literature would then become dominated by successful predictions, and the result would be an inflated measure of our current predictive accuracy.

In an initial publication, we therefore calculated the molecular hydrophobic-to-total volume ratios for a number of molecules. We have subsequently synthesized these molecules and, where possible, solved the crystal structures (see Supporting Information). Because the CSD data was clearest for *l* and *bi* phases, we concentrated predominantly on these systems.

In Figure 4, we show the eight amphiphilic systems with hydrophobic-to-total volume ratio of 40−50% that we later proved able to crystallize. These systems include aromatic polyethers and polyalcohols, aromatic ammonium carboxylates, and cyclohexylammonium carboxylates. On the basis of the results of Table 1, we predicted that these structures would be lamellar or bicontinuous. All eight proved to be lamellar.

In Figure 5, we show the three amphiphilic systems with volume ratios of 20−30%. We predicted that these structures would be predominantly columnar or spherical. Two proved to be columnar, while the third formed as perforated layers. In the latter case, the structure contains pseudo-columns. The results of Figures 4 and 5 taken together show that 10 of the 11 predictions proved correct. This percentage is in keeping with the CSD statistics of Table 1.

We can think of three main caveats to such predictions in general. The first is that we have considered here amphiphilic systems where there are two clear components and where for each component the degree of hydrophobicity (or hydrophilicity) is fairly constant throughout. As we move to more complicated amphiphilic systems, such as triblock systems, there are a greater number of structural architectures.

Second, we have not considered the orientational propensities of the molecular fragments themselves. Certain groups have a preferred orientation with one another. For example, long unbranched aliphatic chains interdigitate in a rodlike fashion. Such parallel interdigitation favors the formation of the lamellar rather than the columnar phase. Thus amphiphilic molecules with unbranched aliphatic chains will have a lamellar structure irrespective of the hydrophobic-to-total volume ratio.

Finally, if the actual domains of the hydrophobic or hydrophilic moieties become so small that contacts are forced between different domains inside the same molecule, then it will no longer be possible to form the simple interfaces envisioned in this Account.[23] As an example, consider the aromatic polyether shown in Figure 6. This molecule has a hydrophobic-to-total volume ratio of 48%, and therefore one might expect a lamellar or bicontinuous structure. But the hydrophobic domains are just single aromatic rings, and the hydrophilic groups are ether functionalities in meta orientation with one another. The meta position allows neighboring hydrophilic moieties on the same molecule to come into contact with one another. As Figure 6 shows, the result is a perforated layer and not a lamellar structure.

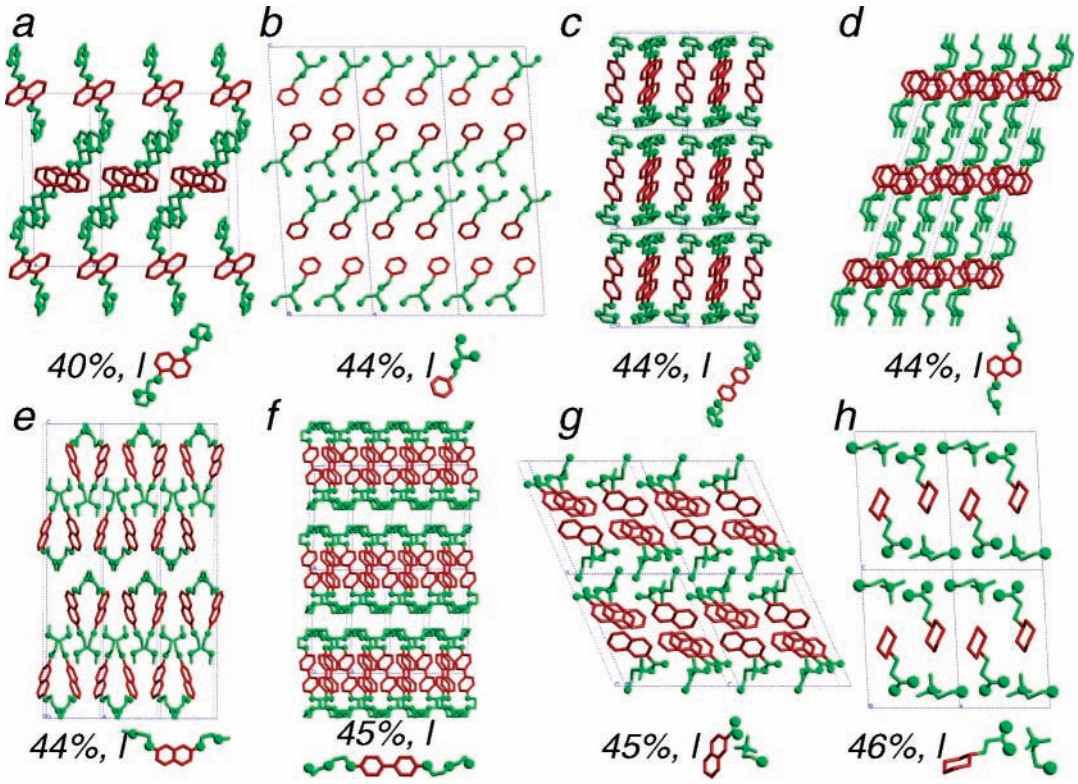

FIGURE 4. Single crystal structures of eight amphiphilic organic molecules previously predicted to have lamellar or bicontinuous topology. For color scheme, see Figure 3. All structures proved to be lamellar.

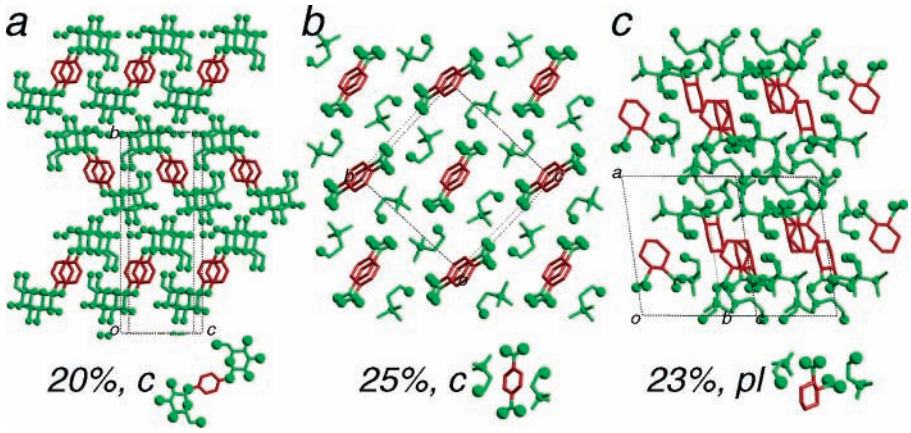

FIGURE 5. Single crystal structures of three amphiphilic organic molecules previously predicted to have a columnar structure. For color scheme, see Figure 3. While structures in panels a and b proved to be columnar, that in panel c did not. In panel c, there are pseudo-columns (in red) running perpendicular to the plane of the paper.

Volume Ratios and Ag Coordination Extended Solids

In recent years, there has been a renewed interest in coordination extended solids (see Supporting Information for further references). In such systems, one typically coordinates metal ions with organic ligands that are multitopic in nature. A multitopic ligand is one where there are multiple ligand groups that readily coordinate to a metal but where, due to the sterics of the molecule, these multiple ligands are forced to coordinate to different metal ions. As metal atoms coordinate to several ligand molecules and ligand molecules coordinate to several metal atoms, the resultant structures contain extended nets, often reminiscent of the structures seen in inorganic chemistry.

In this section of the Account, our attention turns to silver salts coordinated to multitopic ligands. The silver salts have noncoordinating anions such as triflate ($CF_3SO_3^-$), BF_4^-, and SbF_6^-, while the organic multitopic ligands are aromatic nitrile polyether−polyalcohols. Both the metal salt and the organic portions were chosen with some care. Under these conditions, silver is a soft cation—it coordinates readily with the soft aromatic nitriles; the noncoordinating anions are harder—they are often found in

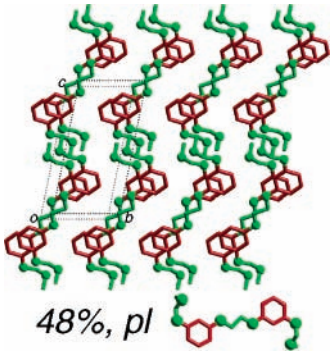

FIGURE 6. Single-crystal structure of an amphiphilic aromatic polyether with small hydrophobic domains. For color scheme, see Figure 3. The meta ether moieties on the same molecule are in close contacts. The result is a perforated lamellar structure type.

the polyether−polyalcohol matrix. We therefore take the silver ions and the aromatic nitrile moieties to form the hydrophobic domain, and the noncoordinating anions together with the polyether−polyalcohol functionalities to be the hydrophilic domain.

In Figure 7, we show the crystal structures of a dozen such systems (see Supporting Information). The structures are given in order of their hydrophobic-to-total volume ratio. In Figure 7a−d, the ratio varies from 21% to 27% and all the structures are columnar. At slightly higher volume ratios, there is a *pl* structure, followed at 34% by a *c* phase, and finally at 35−41%, all structures are either lamellar or bicontinuous. This is the same evolution of structure that we found for both large length scale and small amphiphilic molecules.

Figure 7 is of particular interest because the structures taken together form a kind of static movie showing the topological transformation from the *c* to the *l* structure types. As this figure shows, at low volume ratios the hydrophobic domains, shown in red, form columns each with six columns packed in a hexagon around it (see Figure 7a). As the volume ratio becomes higher, these columns begin to aggregate with one another in pseudo-layers (see Figure 7b−f). At higher concentrations still, these pseudo-layers come together in bona fide lamellar sheets (see Figures 7i,j).

One particular structure of interest is the silver triflate salt with the large tritopic molecule shown in Figure 8a. The core of this molecule, the aromatic nitrile component, has D_{3h} symmetry. The resultant structure is a hexagonal honeycomb planar sheet, where half of the honeycomb nodes are centered on silver ions and half on the tritopic aromatic nitriles (see Figure 8b,c). As Figure 8b further shows, these honeycomb networks dimerize together.

The cavities within the hexagonal holes of these dimerized honeycomb sheets and the spaces between the dimerized sheets are filled with the hydrophilic polyether chains and counterions. The structure can therefore be viewed as a perforated lamellar structure with the perforated sheets composed of the silver−aromatic nitrile net and the hydrophilic portions of the system forming the three-dimensional matrix around these sheets. This is in keeping with a calculated hydrophobic-to-total volume ratio of 29%. This structure therefore is an example of how the amphiphilic structure types shown in Figure 2 adapt themselves to the structural requirements of coordination extended solids.

Trigonal Planar Coordination Extended Solids

The structure shown in Figure 8 hints at two separate themes of amphiphilic coordination extended solids. On one hand, such structures can be understood in terms of volume ratios and the *s*, *c*, *bi*, *pl*, and *l* topologies, while on the other hand their structures are controlled by the topology of the transition metal−multitopic ligand networks themselves.

In this section of the Account, we explore how these themes can work in a cooperative manner. In particular, we seek extended solid topologies that are compatible with the four constant curvature structures, *s*, *c*, *bi*, and *l*. Some thought shows that it is the trigonal planar coordination environment that is especially compatible with these structure types. Fullerenes, carbon nanotubes, and graphite, all composed of trigonal planar atoms, are topologically related to, respectively, the *s*, *c*, and *l* structure types (see Figure 9).

But it is the gyroid structure in which trigonal planar coordination plays its most striking role. As we saw in Figure 1, the gyroid topology is a bicontinuous cubic structure in which there is a zero mean curvature surface between the two domains. The interior of the two domains has, however, a topology like that of a three-dimensional trigonal planar network. These networks are drawn in red and blue in Figure 10. They are referred to as (10,3) networks because they contain ten-member rings of three-coordinate atoms.[24] One such ten-member ring is shown in Figure 10. As can be seen in Figure 10, the (10,3) networks lie at the locus of points furthest away from the gyroid surface itself.

With these geometric relations clear, it is apparent that amphiphilic extended solids composed of tritopic C_{3v} or D_{3h} ligands and trigonal planar transition metal ions are of heightened interest. We therefore examined the CSD for such systems.[25] To limit the scope of the search, we considered ligand molecules where the ligand lone pair was on a nitrogen atom. Because the metal that most often adopts a trigonal planar coordination is the silver ion, we considered only extended solids where this metal ion was coordinated to three nitrogen atoms. The above CSD search revealed 53 such compounds. Forty-five of these compounds contained honeycomb nets, three of the structures can be related to the gyroid topology, and one contains one-dimensional rods (see Supporting Information). Thus the large majority of these structures can be thought to have their origin in the four constant curvature structures.

Twenty-one of the structures involve the organic molecule hexamethylenetetraamine (HMTA),[26,27] an adamantane-shaped ligand shown in Figure 11. This molecule is of T_d symmetry and has four nitrogen atoms, which can potentially coordinate to metal ions. Curiously, in over

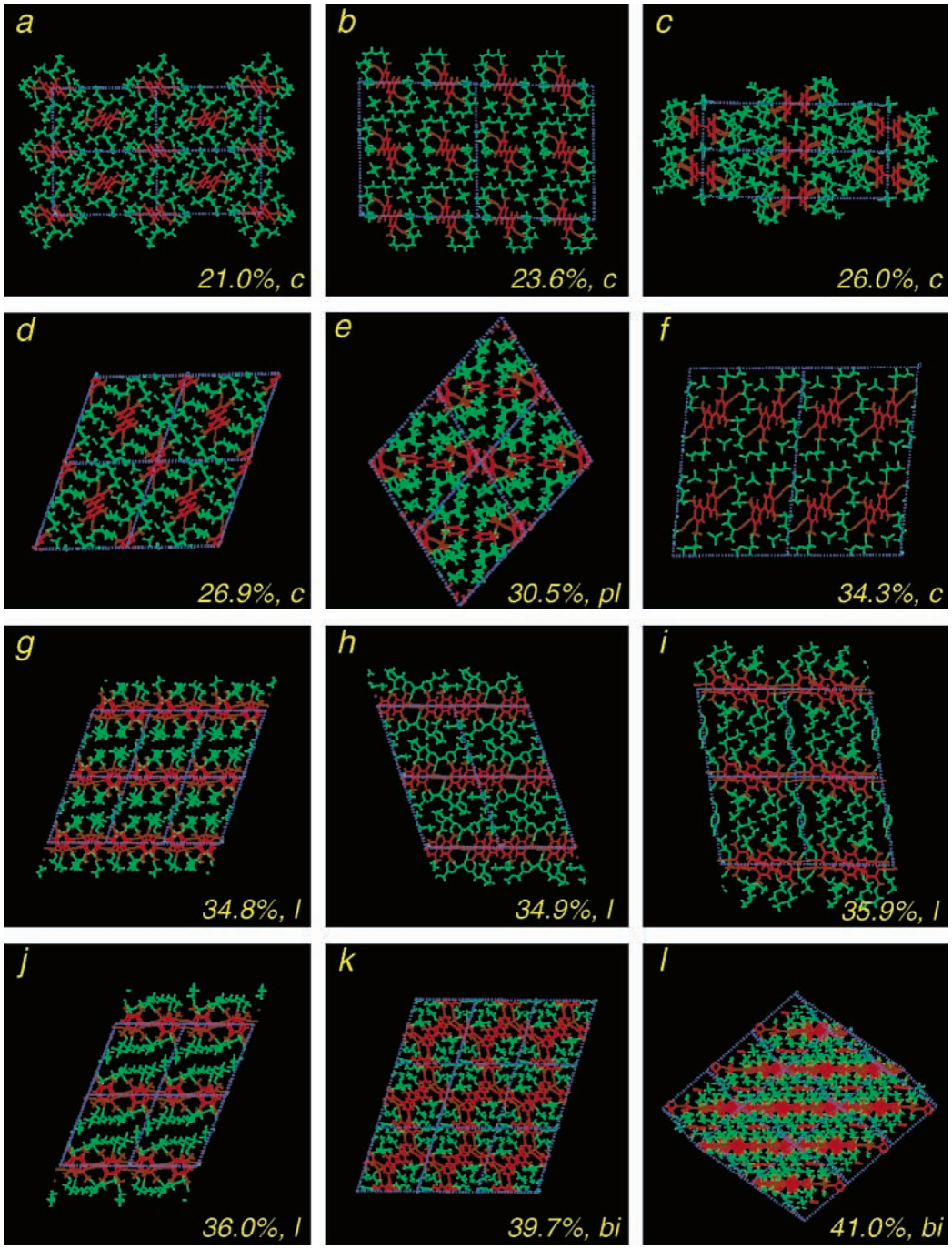

FIGURE 7. Single crystal structures of silver salts of hydrophobic phenylacetylene nitriles with hydrophilic pendant oligo(ethylene oxide) chains. Structures are ordered in increasing hydrophobicity. Hydrophobic, hydrophilic, and intermediate moieties are, respectively, illustrated in red, green, and brown. Also included are hydrophobic-to-total volume fractions and topological types.

three-quarters of the CSD Ag extended solids, only three of the four nitrogen atoms of HMTA are coordinated to silver atoms. As a ligand, HMTA therefore acts effectively as a molecule with C_{3v} symmetry, and we treated it as such in this study.

These 21 HMTA structures show many of the major structural themes in these structures. The honeycomb pattern predominates among them.[28,29] There are variations in this honeycomb pattern. In Figure 12, we show two examples. In both, half the HMTA molecules lie above and half below the honeycomb plane (those above the plane are shown in red; those below in green). The result in both cases is a corrugated honeycomb topology. But in Figure 12a, the raised and lowered HMTA molecules lie in straight lines, while in Figure 12b, they form zigzagged lines. Perpendicular views of the honeycomb sheets are shown in Figure 12c,d.

In Figure 13, we show *ecitit*, Ag(HMTA)(4-nitrobenzoate)·2.5H_2O, and *eciviv*, Ag(HMTA)(2-naphthoxyacetate)·(H_2O)(C_2H_5OH).[27] In both structures, the silver·HMTA network has a honeycomb topology with half the nodes of the honeycomb centered on silver ions and half on HMTA molecules. In Figure 13a,c, the honeycomb sheets, in red, are given in a sideview. As a comparison to the

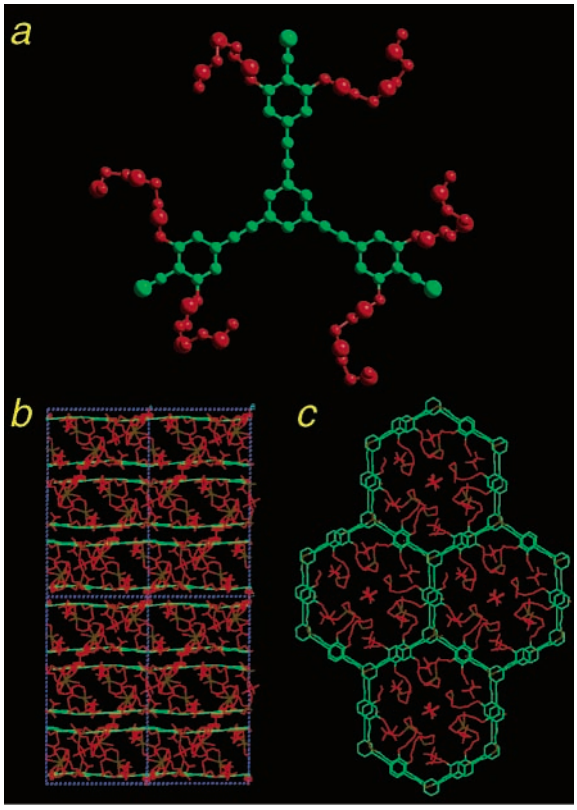

FIGURE 8. Panel a shows the molecular framework of a tritopic phenylacetylene nitrile ligand with six pendant tri(ethylene oxide) chains: large red spheres, oxygen atoms; large green spheres, nitrogen atoms; small red and green spheres, carbon atoms. Panel b shows a view down the [1 0 0] direction. Panel c shows a view down the *c* axis of a single bilayer. For color scheme, see Figure 7.

sideviews of Figure 12c,d shows, in *ecitit* and *eciviv*, the honeycomb sheets are, respectively, in the types of Figure 12c,d. Figure 13a,c shows that counterions and solvent molecules lie sandwiched between the honeycomb sheets. Viewed this way, *ecitit* and *eciviv* both have *l* topology.

This structural view contrasts itself with the picture of the previous sections. There we divided the domains of the molecules by the hydrophilicity of the various functional groups. Going back to this picture, the carboxylate and amine functionalities are hydrophilic; the aromatic rings are hydrophobic. We follow our previous work, and consider all sp^3 carbon atoms bonded to an oxygen or an amine nitrogen to be hydrophilic. Because the silver ions in HMTA salts are coordinated to only the hydrophilic carboxylate or amine groups, they are considered to be hydrophilic.

The above definitions lead to a different picture of the overall topologies. We redraw the structures of *ecitit* and *eciviv* with the hydrophilic and hydrophobic portions in, respectively, green and red. The structure of *ecitit* is redrawn in Figure 13b: it is now columnar. The structure of *eciviv* is redrawn in 13d: it remains lamellar. Calculations of the hydrophobic-to-total volume ratio are, respectively, 23.3% and 35.7%, in keeping with these topological findings.

Similar results are found for the other systems in this CSD search and in other tritopic silver salts that we have prepared. Constant curvature structures therefore play a dual role in three-coordinate extended solids. On one hand, the coordination extended networks adopt constant curvature topologies. At the same time, those systems that are amphiphilic divide their hydrophobic and hydrophilic parts into constant curvature topologies, topologies that may differ from the topology of the extended nets themselves.

We may also learn about constant curvature structures from another Ag·HMTA system, *ziwtii*,[26] $AgPF_6$·HMTA·H_2O. Its structure is shown in Figure 14. As this figure shows, the Ag ions and HMTA molecules form one three-dimensional network, and the PF_6^- ions and H_2O molecules, hydrogen-bonded (dotted blue lines) to each other, form another.

Figure 14 shows that both the Ag·HMTA networks and the PF_6^- ions and H_2O molecules adopt topologically similar nets: both have (10,3) topology. The resultant structure is related to the gyroid structure. The relation between the gyroid and *ziwtii* structure is shown in Figure 14b,c. Both structures are cubic, but the gyroid has body-centered symmetry, while *ziwtii* is distorted away from this geometry and is primitive cubic. *Ziwtii* therefore represents a striking example of a gyroid-type structure in which the Ag·HMTA network forms one domain and the PF_6^- ions and H_2O molecules the other.

Doubly Interpenetrated Networks of Gyroid Type

A number of other systems contain (10,3) nets, among them (by CSD codename) *cafrux*, *huyker*, *paqdeq*, *putyae*, *qithac*, *rizhut*, *tasfau*, *tashuq*, *xehxox*, *yapnuy*, and *zuqvem* (see Supporting Information). All these structures are beautiful. We restrict our attention here to systems with doubly interpenetrated (10,3) nets such as those found in the gyroid topology (note that in the gyroid topology the two (10,3) nets have opposite chiralities). In these systems, the utility of the gyroid topology in understanding the final structure is most clear. We consider first the silver salt that we recently prepared containing 5-(4-ethynyl pyridine)pyrimidine, EPP, see Figure 11. The composition of this crystal is Ag·BF_4·EPP. This structure contains two (10,3) networks composed of the Ag·EPP moieties. These networks are illustrated in Figure 15a. As this figure shows, these networks can be directly compared to the gyroid networks shown in Figure 10.

If the silver·EPP net adopts the (10,3) networks of the gyroid structure, what role does the gyroid surface, shown in Figures 1 and 10, play in the full crystal structure? The answer lies in the BF_4^- anions. In Figure 15b, we draw the gyroid surface (adapted to the tetragonal metric of the crystal) together with the BF_4^- anions. This figure shows that the anions lie near the gyroid surface itself. As in the previous section, the silver·organic net forms one component of a constant curvature structure; the anions form another.

With this in mind, we turn to *mubqij*,[30] a silver salt involving diquioxalino[2,3-*a*:2′3′-*c*]phenazine, DQP, see

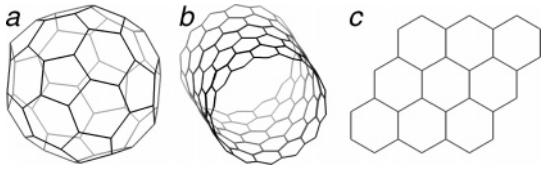

FIGURE 9. Trigonal nodal frameworks of (a) spherical fullerene, (b) columnar carbon nanotubes, and (c) lamellar graphite.

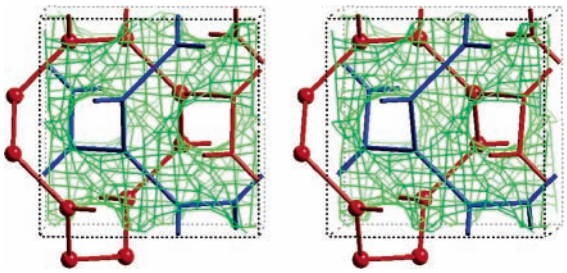

FIGURE 10. Stereoview of the gyroid surface and (10,3) networks along the cubic [1 0 0] direction: surface, green; trigonal networks, red and blue. Vertices of one ten-member ring are given as red spheres.

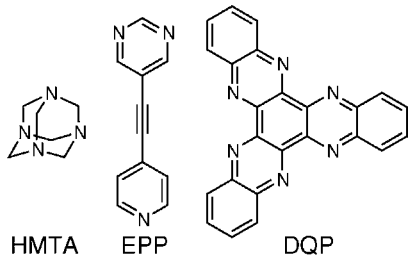

FIGURE 11. Chemical structures of hexamethylenetetraamine (HMTA), 5-(4-ethynyl pyridine)pyrimidine (EPP), and diquioxalino-[2,3-*a*:2′3′-*c*]phenazine (DQP).

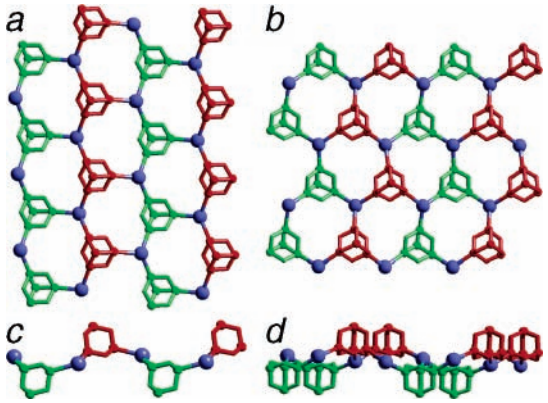

FIGURE 12. Two different types of honeycomb patterns formed by Ag·HMTA: (a,b) view of honeycomb net; (c,d) perpendicular views to views in panels a and b. HMTA molecules raised above the honeycomb plane are in red; those below the plane are in green; silver atoms in the honeycomb plane are large blue spheres; nitrogen atoms are small red and green spheres.

Figure 11. Its chemical formula is $Ag_3(DQP)_2{\cdot}(NO_3)_3(CH_2Cl_2)_3(H_2O)_3$. It is the only other clear double (10,3) net structure of which we know.[31] The silver·organic net of *mubqij* is shown in Figure 16a.[32] In Figure 16b, we draw the gyroid topology adapted to the hexagonal unit cell of *mubqij*. As in the previous example, we see that the two (10,3) nets have the same topology as the gyroid networks.

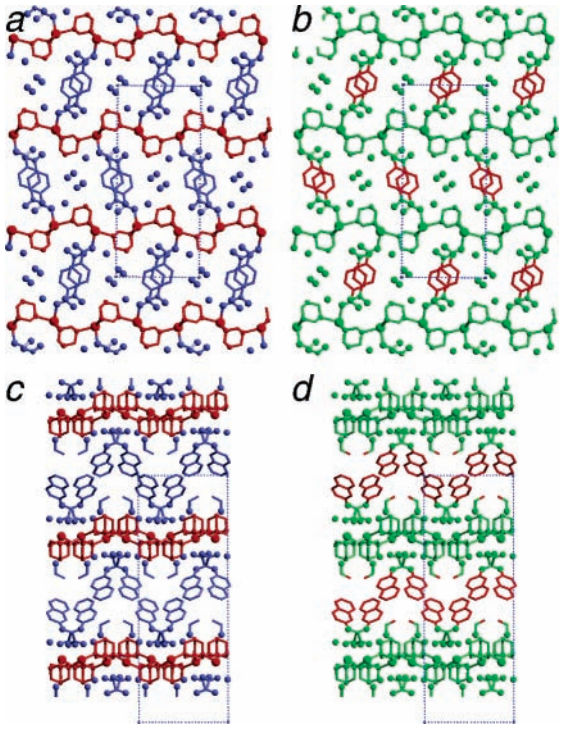

FIGURE 13. CSD structures of (a,b) *ecitit* and (c,d) *eciviv*:[27] (a) *ecitit*'s Ag·HMTA honeycomb networks are red; counterions and solvent molecules are blue; (b) *ecitit*'s hydrophilic domains are green; hydrophobic aromatic portions are red; (c,d) same color schemes are used for *eciviv*. For honeycombs presented in side-view, see Figure 12. Large spheres denote silver atoms; medium spheres denote oxygen atoms; small spheres denote nitrogen atoms. *Ecitit* with color scheme in panel a is lamellar, while in panel b, it is columnar. *Eciviv* is lamellar in both panels c and d.

In Figure 16c, we show the gyroid surface together with the NO_3^- anions and solvent molecules. As this figure shows, like Ag·BF_4·EPP, the anions and solvent molecules adhere to the gyroid surface itself.

In the structures shown in Figures 15 and 16, not only do the anions adhere to the gyroid interface, but there also appears to be a relation between the symmetry of the anion and the high symmetry points of the gyroid interface itself. The gyroid surface has two points of higher symmetry. They are of S_4 and S_6 symmetry. In the first structure discussed, the anions are BF_4^- ions. Such ions are of T_d symmetry. While S_4 is a subgroup of T_d, S_6 is not. Interestingly, the BF_4^- ions in the former structure are found near the S_4 sites.

In the latter structure, *mubqij*, the anions are NO_3^- ions. Pairs of these anions are related to each other by an inversion center leading to dimers of overall D_{3d} symmetry (in Figure 16, one such pair can be seen near the special point ($^1/_3$, $^2/_3$, $^2/_3$)). S_6 is a subgroup of D_{3d}; S_4 is not. As in

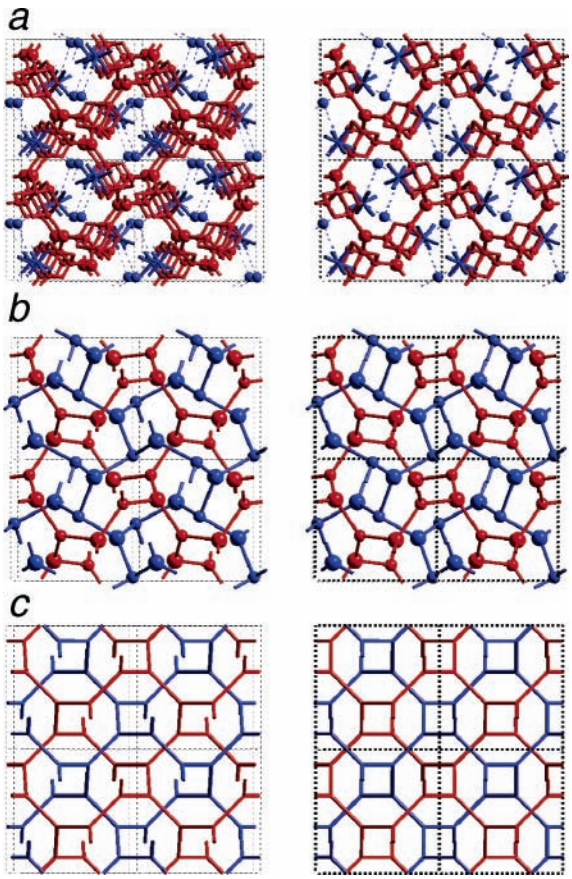

FIGURE 14. Panel a shows a stereoview of the CSD crystal structure of Ag·HMTA salt, *ziwtii*:[26] Silver atoms and HMTA molecules, red; PF_6^- ions and H_2O molecules, blue; coordination and covalent bonds, solid lines; hydrogen bonds, dotted blue lines; large red spheres, silver atoms; small red spheres, nitrogen atoms; blue spheres, oxygen atoms; hydrogen atoms not shown. Panel b shows a schematic stereoview representation of *ziwtii*: HMTA molecules, large red spheres; silver atoms, small red spheres; PF_6^- ions, large blue spheres; H_2O molecules, small blue spheres; coordination and hydrogen bonds, lines. Panel c shows a stereoview of the gyroid network structure. The view in panel c may be directly compared to view in panel b.

the previous system, the site with compatible symmetry to the anions (in this case, the S_6 sites) has pairs of anions near it; the other site (in this case, that of S_4 symmetry) does not.

Although it is difficult to extrapolate from these examples, it is possible that the alignment between anion and gyroid surface symmetries is not accidental. If so, we can imagine that the gyroid structure is partially stabilized by these symmetry considerations. This factor alone though is not enough to ensure a gyroid vs lamellar topology: as the CSD search discussed in the previous section shows, the lamellar topology is much more common than the gyroid topology.

Taken together, the role of constant curvature is clear. The geometries in Figures 15 and 16 are complex. While we could have seen the (10,3) patterns in these two structures without reference to the gyroid topology, we would then have not been able to rationalize the anion positions. As in our previously discussed results on

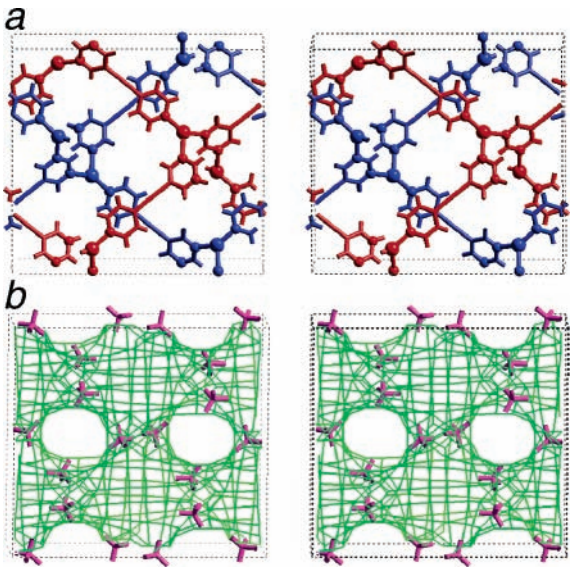

FIGURE 15. Stereoviews of $AgBF_4$·EPP. Panel a shows the single crystal structure along the orthorhombic [0 1 0] axis: interpenetrating networks, red and blue; large spheres, silver atoms; small spheres, nitrogen atoms. Panel b depicts the gyroid surface metrically adapted to the orthorhombic cell of $AgBF_4$·EPP and BF_4^- counterions of the crystal structure: surface, green; BF_4^- counterions, magenta. Counterions adhere to the gyroid surface.

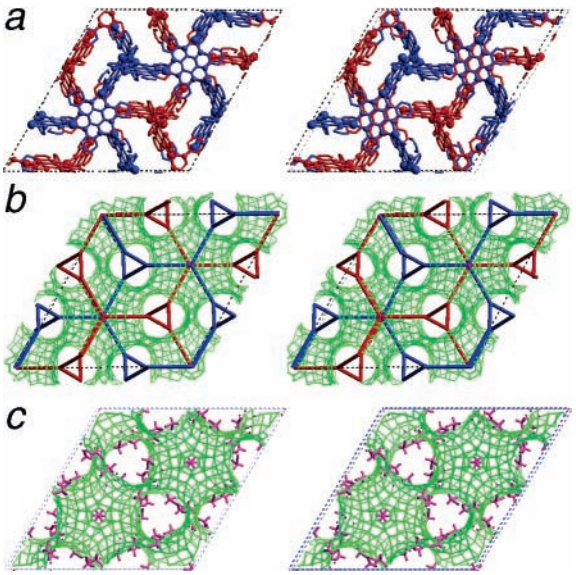

FIGURE 16. Stereoviews of (a) the CSD crystal structure *mubqij*[30] (for color scheme, see Figure 15), (b) the gyroid structure given with reference to a hexagonal cell ((10,3) networks, red and blue; interfacial surface, green), and (c) the gyroid surface adapted to the hexagonally metric cell of *mubqij* together with the NO_3^- counterions and solvent molecules of *mubqij* (surface, green; counterions and solvent, magenta). Counterions and solvent molecules adhere to the gyroid surface.

hydrophobic-to-total volume ratios, the utility of constant curvature topologies in understanding small molecule amphiphilic and three-coordinate extended solid structures is evident.

This work was supported by the National Science Foundation (Grants DMR-0104267 and CHE-0209934). We have had the good

fortune in the past few years to work with Jeffrey Moore, D. Venkataraman, Geoff Gardner, Wonyoung Choe, and Yuan-Hon Kiang. More than any others, it has been their laboratory results that have led us to the research reported in this Account.

Supporting Information Available: Synthetic methods, crystallographic descriptions, tables of predicted and observed volume ratios and topologies, crystal refinement data, bond distances, bond angles, and anisotropic thermal factors for compounds shown in Figures 4b,c,e and 6, experimental and calculated powder diffraction data for the above compounds, and additional references. This material is available free of charge via the Internet at http://pubs.acs.org.

References

(1) Kitaigorodsky, A. I. *Molecular Crystals and Molecules*; Academic Press: New York, 1973.

(2) Maddox, J. Crystals from First Principles. *Nature (London)* **1988**, *335*, 201−201.

(3) Andersson, S. On the Description of Complex Inorganic Crystal Structures. *Angew. Chem., Int. Ed. Engl.* **1983**, *22*, 69−81. See Supporting Information.

(4) Buckingham, A. D.; Fowler, P. W. Do Electrostatic Interactions Predict Structures of van der Waals Molecules? *J. Chem. Phys.* **1983**, *79*, 6426−6428.

(5) Stone, A. J. *The Theory of Intermolecular Forces*; Claredon Press: Oxford, U.K., 1996. See Supporting Information.

(6) Beyer, T. Lewis, T.; Price, S. L. Which Organic Crystal Structures are Predictable by Lattice Energy Minimisation? *CrystEngComm* **2001**, *3*, 178−213. See Supporting Information.

(7) Hamley, I. W. *The Physics of Block Copolymers*; Oxford University Press: New York, 1998.

(8) Khandpur, A. K.; Förster, S.; Bates, F. S.; Hamley, I. W.; Ryan, A. J.; Bras, W.; Almdal, K.; Mortensen, K. Polyisoprene-Polystyrene Diblock Copolymer Phase Diagram Near the Order−Disorder Transition. *Macromolecules* **1995**, *28*, 8796−8806. See Supporting Information.

(9) Borisch, K.; Diele, S.; Göring, P.; Müller, H.; Tschierske, C. Amphiphilic N-benzoyl-1-amino-1-deoxy-D-glucitol Derivatives Forming Thermotropic Lamellar, Columnar and Different Types of Cubic Mesophases. *Liq. Cryst.* **1997**, *22*, 427−443. See Supporting Information.

(10) von Schnering, H. G.; Nesper, R. How Nature Adapts Chemical Structures to Curved Surfaces. *Angew. Chem., Int. Ed. Engl.* **1987**, *26*, 1059−1080.

(11) Andersson, S. Hyde, S. T.; Larsson, K.; Lidin, S. Minimal-Surfaces and Structures-from Inorganic and Metal Crystals to Cell-Membranes and Bio-Polymers. *Chem. Rev.* **1988**, *88*, 221−242. See Supporting Information.

(12) Gunning, B. E. S. Greening Process in Plastids. 1. Structure of Prolamellar Body. *Protoplasma* **1965**, *60*, 111−130.

(13) Hyde, S. T.; Ninham, B.; Andersson, S.; Blum, Z.; Landh, T.; Larsson, K.; Lidin, S. *The Language of Shape*; Elsevier: Amsterdam, 1997.

(14) Luzzati, V.; Spegt, P. A. Polymorphism of Lipids. *Nature (London)* **1967**, *215*, 701−704. See Supporting Information.

(15) Hajduk, D. A. Harper, P. E.; Gruner, S. M.; Honeker, C. C.; Thomas, E. L.; Fetters, L. J. A Reevaluation of Bicontinuous Cubic Phases in Starblock Copolymers. *Macromolecules* **1995**, *28*, 2570−2573.

(16) Flory, P. J. *Principles of Polymer Chemistry*; Cornell University Press: Ithaca, NY, 1953.

(17) No inverted lamellar or bicontinuous phase exists: in these structures, the hydrophobic and hydrophilic domains have exactly the same shape.

(18) Note that van der Waals radii indicate the distances at which van der Waals attractive energy terms are in equilibrium with shorter range interatomic repulsive forces. Therefore van der Waals radii themselves form a lower limit for the distances at which van der Waals attractions become dominant. We find that multiplicative factors of 1.15−1.30 times the van der Waals radii give structural topologies in closest agreement with the visual appearance of the different unit cells.

(19) Owen, J. D. Crystal Structure of Two Bridged Macrobicyclic Polyethers- 1,5,12,16,23,26,29-Heptaoxa[73,14][5.5]orthocyclophane and 1,5,12,16,23,26,29,32-Octaoxa[103,14][5.5]orthocyclophane. *J. Chem. Soc., Perkin Trans. 2* **1981**, 12−18.

(20) Frydenvang, K.; Hjelvang, G.; Jensen, B.; Do Rosario, S. M. M. Structures of the Choline Ion in Different Crystal Surroundings. *Acta Crystallogr., Sect. C: Cryst. Struct. Commun.* **1994**, *50*, 617−623.

(21) Grabarnik, M.; Goldberg, I.; Fuchs, B. A New Class of Chiral Macrocyclic Polythiacrown Systems and a Caveat. *J. Chem. Soc., Perkin Trans. 1* **1997**, 3123−3125.

(22) Graingeot, V.; Brigando, C.; Benlian, D. 2,4,6-Tri-O-benzyl-myo-inositol. *Acta Crystallogr., Sect. C: Cryst. Struct. Commun.* **1996**, *52*, 2283−2285.

(23) This point is clear to us in hindsight. In an earlier publication (see Supporting Information), we made a few predictions based on small-scale domain amphiphilic systems with meta-substituted aromatic rings. In view of our new insight, we withdraw these predictions.

(24) Wells, A. F. *Three-Dimensional Nets and Polyhedra*. Wiley: New York, 1977.

(25) Statistics were taken from Cambridge Structural Database, version 5.25 (298 097 structures, November 2003 release).

(26) Carlucci, L.; Ciani, G.; Proserpio, D. M.; Sironi, A. A Three-Dimensional, Three-Connected Cubic Network of the $SrSi_2$ Topological Type in Coordination Polymer Chemistry: [Ag(hmt)]-$(PF_6)\cdot H_2O$ (hmt = hexamethylenetetramine). *J. Am. Chem. Soc.* **1995**, *117*, 12861−12862.

(27) Zheng, S.-L.; Tong, M.-L.; Fu, R.-W.; Chen, X.-M.; Ng, S.-W. Toward Designed Assembly of Microporous Coordination Networks Constructed from Silver(I)-Hexamethylenetetramine Layers. *Inorg. Chem.* **2001**, *40*, 3562−3569.

(28) Of the 21 structures, 20 adopt a honeycomb sheet structure; the last, as we discuss herein has a cubic (10,3) net topology.

(29) The preference for the honeycomb structures is mirrored in the inorganic database. The Pearson compendium of intermetallic systems cites 327 phases with the AlB_2 structure type (a structure based on honeycomb sheets) but only six with the $SrSi_2$ structure type (a structure with (10,3) nets). Interestingly, the Pearson database also cites extensively a third trigonal planar structure, $ThSi_2$. Although Pearson gives 88 examples of this structure type, our CSD search showed only one had this topology.

(30) Bu, X.-H.; Biradha, K.; Yamaguchi, T.; Nishimura, M.; Ito, T.; Tanaka, K.; Shionoya, M. A Novel Polymeric Ag(I) Complex Consisting of Two Three-Dimensional Networks which are Enantiomeric and Interpenetrating. *Chem. Commun.* **2000**, 1953−1954.

(31) *Tashuq* also has two (10,3) networks, but the overall structure is sufficiently distorted that we do not consider it here.

(32) A second isotypical structure has been reported; its full structure is not given.[30]

AR0401653